# Combinatorial effect of imiquimod and bevacizumab on carcinoma cell and cancer stem cells in hamster buccal pouch carcinogenesis

**Amr Mahmoud Mohamed**
Department of Oral and Dental Pathology, Faculty of Dental Medicine, Al-Azhar University, Cairo, Egypt
amrmohamed.209@azhar.edu.eg

**Emad Soliman Mohammed Al-qalshy**
Department of Oral and Dental Pathology, Faculty of Dental Medicine, Al-Azhar University, Cairo, Egypt
emadalqalshy.209@azhar.edu.eg

**Bakheet Elkot Mostafa Elsadek**
Department of Biochemistry and Molecular Biology, Faculty of Pharmacy, (Boys-Assiut), Al-Azhar University, Egypt.
bakheet.elkot@azhar.edu.eg

**Mohamed Gomaa Attia Zouair**
Department of Oral and Dental Pathology, Faculty of Dental Medicine, Al-Azhar University, Cairo, Egypt
mohamedzouair.209@azhar.edu.eg

***Corresponding author: Emad Alqalshy,** emadalqalshy.209@azhar.edu.eg

## Abstract

1) Background: The aim of the present study was directed to investigate the effect of imiquimod and bevacizumab on cancer stem cell(s) (CSC(s)) of induced hamster buccal pouch (HBP) carcinoma; 2) Methods: 50 syrian male hamsters were divided into 5 group(s) (G(s)),10 each. While the animals in GI (negative control) were, left untreated for 19 weeks (ws), the right pouches of those in (GII- GV) were painted with 7,12-dimethylbenz (a) anthracene (DMBA), 3times a week for 14 ws. After that, the animals in GII (positive control) were left with no additional treatment for other 5 ws (total period 19 ws), whereas those in GIII were painted with imiquimod once daily for other 4 ws, then, after other week (total period 19 ws) the animals were euthanized. Those in GIV were injected intraperitoneally (IP) with bevacizumab (10mg/kg / once daily for a week), then, after other week (total period 16 ws) the animals were euthanized and those in GV were painted with imiquimod and IP injection with bevacizumab with doses and administration method similar to those introduced in single treatments then, after other week (total period 19 ws) the animals were euthanized. After termination of the experiment, gross observations and tumor volume were recorded, then, the animals were euthanized, and all right pouches were surgically excised, prepared, fixed and processed for hematoxylin and eosin (H&E) stain examination for recording histopathological features including the depth of invasion (DOI) and immunohistochemical (IHC) staining utilizing B-lymphoma moloney murine insertion region (BMI-1) stem cell marker and vascular endothelial growth factor (VEGF) antibody.; 3) Results: : tumor volume recorded highly significant difference (p value < 0.001) between GIII, GIV or GV and GII. Histopathological findings revealed DOI with highly significant difference (p value < 0.001) between GIII, GIV or GV and GII. BMI-1 and VEGF antibodies revealed highly significant difference (p-value < 0.001) between GV and the following; GIII and GIV consequently. In contrast, BMI-1 had non-significant difference (p-value < 0.125) between GIII and GIV, while VEGF had highly significant difference (p-value < 0.001) between GIII and GIV; 4) Conclusion: bevacizumab could inhibit tumor vasculature-VEGF expression. Imiquimod could inhibit CSCs-BMI-1 expression. Combination of imiquimod-bevacizumab has an inhibitory effect on carcinoma cell and cancer stem cells in HBP SCC.

**Keywords:** HBP carcinoma; imiquimod; bevacizumab; CSCs.

**DOI Number: 10.14704/nq.2022.20.13.NQ88083** **NeuroQuantology 2022; 20(13): 619-634**

## Introduction

Oral squamous cell carcinoma (OSCC) is an aggressive and insidious malignancy covering the lips or other parts of the oral cavity(1). It was estimated that about 300,000 new cases were diagnosed as OSCC and about 150,000 cases were died from OSCC in 2020, accounting for almost 2% of new cases and deaths in total 36 cancers(1). 7,12-dimethylbenz (a) anthracene (DMBA) is commonly utilized as a major carcinogen to develop tumors in the hamster buccal pouch (HBP) of golden Syrian hamsters, DMBA causes neoplasm by inducing severe inflammation and dysplasia in the buccal pouches as well as by causing extensive oxidative damage to DNA. The process begins as systemic debilitation of the animals, perioral alterations, decrease in the pouch length as a result of necrosis in the distal end of the pouch and end by HBP tumor growth(2-13).

Cancer stem cells (CSC(s)) are known as cells that show self-renewal ability and asymmetric division. These cells are also associated with cancer cell growths and metastasis and tumor recurrence following treatment. Studies have recently shown that targeting CSCs can be an effective treatment strategy for cancer treatment(11, 14). CSC markers that could have potential usefulness within therapeutic, diagnostic, and prognostic approaches are pointed out and focus on deadliest tumors as OSCC(15).

Many CSC markers have been utilized, amongst the most common and most studied are aldehyde dehydrogenase A1 (ALDH1), cluster of differentiation 44 (CD44), and B-lymphoma moloney murine insertion region (BMI-1). BMI-1 acts in the self-renewal ability of stem cells. High expression of BMI-1 in cancer was related to epithelial–mesenchymal transition and poor prognosis. BMI has been demonstrated to be involved in multiple biological processes, such as embryonic development, organ formation, tumorigenesis, stem cells stabilization, and differentiation(16, 17).

Many studies have shown that BMI-1 expression is frequently upregulated in various types of human cancers, including OSCC, acute myeloid leukemia, nasopharyngeal carcinoma and many other types of cancer which indicates that BMI-1 might play important roles in cancer initiation and progression(18-30). Angiogenesis has been identified as an important determinant of solid tumor growth and metastasis. Several regulatory factors are involved in tumor angiogenesis, among which vascular endothelial growth factor (VEGF) serves a particularly important role so, the usefulness of angiogenesis and its relative markers on human as well as experimental oral carcinogenesis has been a matter of interest by various investigators(31-38). Bevacizumab, a monoclonal antibody targeted drug which directly binds to VEGF-A around the tumor and inhibits tumor angiogenesis. Moreover, bevacizumab exerts an antitumor effect by inhibiting the nutrient supply to tumor cells and thought to cause regression of existing tumor vasculature and prevent the development of new blood vessels, thereby inhibiting tumor growth(31, 35, 39). Bevacizumab is approved by food and drug administration (FDA) and is successfully used in many types of cancers either alone or in combination with other chemotherapy drugs and radiotherapy(40-44).

In addition to its function as an antiangiogenic agent, bevacizumab immunomodulatory properties have likely played a role in its clinical activity. The durable clinical benefit seen with immune checkpoint inhibitors across a wide range of cancer types underscores the significance of effective anticancer immunity(45-48).

Imilquimod is an immune response modifier that acts as a Toll-like receptor-7 (TLR-7) agonist which induces cytokines, starting an inflammatory skin or mucosal reaction directed primarily against malignant or virus-infected cells, and has virtually no effect on normal skin or mucosa(49-53).

Imiquimod 5% cream is licensed in the United States FDA and Europe (EMA) for the treatment of external genital warts, superficial basal cell carcinoma, actinic keratitis, and is being experimentally used in various other dermato-oncological conditions(54-58), oral dysplastic lesions or oral cancers(59-62).

Hence, the main target of the present study was to assess the effects of imiquimod and/or bevacizumab on DMBA induced HBP carcinoma. The assessment was based on the animal's general health examinations, HBP gross observations, histological tumor tissue changes and IHC examinations.

## Materials and Methods

### *Chemicals*

DMBA (0.5%) was obtained from Sigma-Aldrich company, dissolved in paraffin oil. Imiquimod A topical cream formulation containing 5% Imiquimod marketed

by 3M pharmaceuticals as Aldara. Bevacizumab (trade name Avastin) was obtained from Roche company dissolved in 0.9% sodium chloride (10 mg/ml)(63).

*Animals*

50 Syrian male hamsters, 5 weeks (ws) old, weighing 80-120g were obtained from the animal house, Cairo University, Cairo, Egypt. A healthy hamster had normal, smooth gait, bright, clear eyes, healthy skin and soft, shiny coat that free of dry patches, parasites, cuts and swellings.

The animals were kept in a separate and labelled cages and allowed to live in optimal conditions under the supervision of the staff members of military veterinary hospital according to the protocol by the local ethical committee (Ethical Code No. 148/164, 30-04-2019).

*Experimental design*

After a week of adaptation, the animals were divided randomly into 5 group(s) (G(s)),10 each. While the animals in GI (negative control) were, left untreated, the right pouches of those in GII, GIII, GIV and GV were painted with the 0.5% DMBA in liquid paraffin using a number 4 camel hair brush, 3 times a week for 14 ws(64). After that, the animals in GII (positive control) were left with no additional treatment for other 5 ws (total period 19 ws), while those in GIII (imiquimod), painted with imiquimod to the injured buccal pouch once daily for other 4 ws(65), after one week (total period 19 ws), the animals of this group were euthanized.

The animals in GIV (bevacizumab) were injected IP by insulin syringe with VEGF inhibitor (Bevacizumab), via IP injection once daily for a week(66), after one week (total period 16 ws), the animals of this group were euthanized, while those in GV (imiquimod-bevacizuumab) animals received a combination of imiquimod and bevacizumab with doses and administration method similar to those introduced in single treatments, then after one week (total period 19 ws), the animals of this group were euthanized.

*General health examinations:*

During the experiment, the changes in the animal's general health were recorded. Hamsters showed one or more of these signs if they were coping with illness or injury: loss of appetite, inactivity, huddling in a corner, sneezing, wheezing, and/or discharge from the nose or eyes, wetness around the tail, diarrhea and hair loss.

*Tumor volume measurement*

After termination of the experiment, gross observations were recorded (mucosal thickness, exudation, ulcers, and tumors.), the animals were euthanized, the right cheek pouch was everted, and the diameter of each tumor was measured with a Vernier caliper **(Fig. 1).** The tumor volume was calculated by the formula, Vmm3 = (4/3) π [(D1/2) (D2/2) (D3/2)], where D1(Hight), D2(width) and D3 (length) are the three diameters (mm) of the tumor(67).

**Fig. (1):** Calculating tumor volume using Vernier caliper

*Histopathological examinations:*

The fixed specimens were dehydrated in an ascending ethanol series, embedded in paraffin wax to form paraffin blocks. Tissue sections of 4µm thickness were cut using rotary microtome, mounted on glass slides, processed, and stained with H&E for light microscopic examination.

*Measurement of the depth of invasion (DOI):*

DOI was measured for all surgical specimens based on the H&E section. DOI was measured from the basement membrane of the surface epithelium to the deepest point of tumor nest. It has further been classified as less invasive ≤5 mm, moderate invasive 6–10 mm, and deeply invasive ≥10 mm, according to American Joint Committee on Cancer (AJCC)(68) **(Fig. 2)**.

DOI was measured using Leica QWIN V3 image analyzer computer system (Switzerland), controlled by Leica QWIN V3 software, oral and dental pathology department, Faculty of Dental Medicine (Boys- Cairo), Al-Azhar University, Egypt.

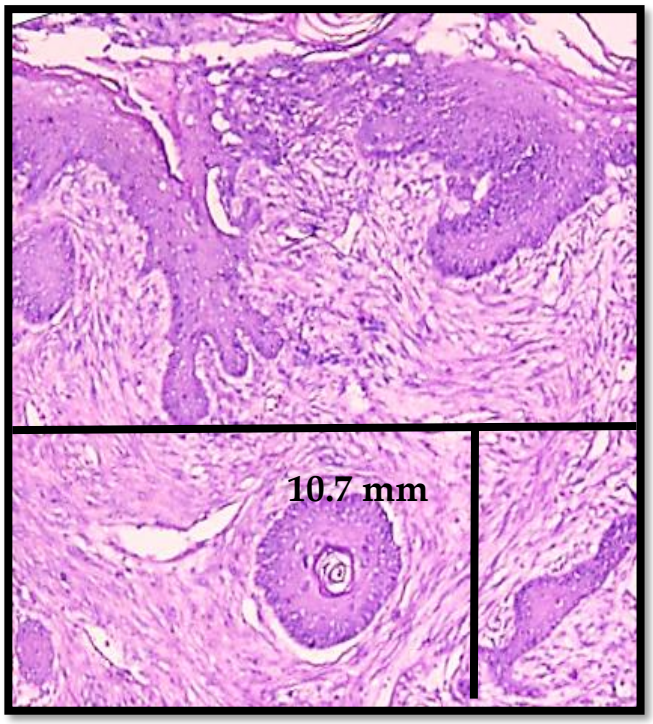


**Fig. (2):** Photograph of measuring the DOI, the greatest invasion was measured by dropping a "plumb line" from the horizon to the deepest invasive nest.

*Immunohistochemical examination:*

Other tissue sections were cut at 4µm and put on positive charged slides for the application of standard labeled streptavidin- biotin method to demonstrate the expression of BMI-1 & VEGF antibodies. The sections were deparaffinized in xylene and rehydrated through graded ethanol (100%, 95 % and 70 %) each run for 5 minutes. Slides were washed in distilled water then in phosphate buffered saline (PBS), each for 5 minutes. Endogenous peroxidase activity was blocked using 3% solution of hydrogen peroxide (H2O2) in methanol for 30 minutes at room temperature. Slides were then washed in PBS. Slides were then immersed in plastic jars containing 200 ml of citrate buffer (pH 6). The jars were put in microwave at maximum power at 100°C for 3 intervals, each one 5 minutes. Slides were left at room temperature to coal gradually. Slides were then washed in distilled water followed by PBS for 5 minutes. Tissue sections were received one or two drops of the primary antibodies (BMI-1 & VEGF) in a dilution of 1:100 and incubated in a humid chamber at room temperature overnight. Slides were then washed in distilled water, followed by PBS for 5 minutes. Biotinylated secondary antibody was added and incubated at room temperature for 30 minutes. Tissue sections were then washed in PBS for 5 minutes. One or two drops of peroxidase-labeled streptavidin were applied for 30 minutes at room temperature then washed in PBS. The tissue sections were received DAB for 2-4 minutes to develop color, followed by putting in distilled water. Tissue sections were counterstained using Mayer hematoxylin for one minute and then washed in tap water. The slides were placed in two changes of 95% alcohol followed by two changes of absolute alcohol, each for 3 minutes then mounted with DPX and covered with plastic covers in order to be examined. Negative controls were prepared by omitting the primary antibody. Liver tissues and breast carcinoma were used as positive controls for VEGF and BMI-1 respectively.

The immunostained sections were examined using light microscope to assess the prevalence of positive cases and the localization of immunostaining within the tissues. In addition, image analysis computer system was used to assess area percentage of BMI-1 and VEGF positive cells of the immunostaining. Assessments were selected under a low power lens (10×10), then counting was conducted under a high-power lens (10 ×40), and a mean value was chosen for statistical analysis(69).This was done in Oral and Dental Pathology Department, Faculty of Dental Medicine (Boys-Cairo), Al-Azhar University, Egypt.

*Statistical analysis:*

The results were recorded as the mean ± standard deviation (SD) and statistically analyzed. A one-way analysis of variance (ANOVA) was performed using SPSS version 17.0 for windows. The comparison between more than two independent groups with quantitative data and parametric distribution was done by using ANOVA followed by post hoc analysis using LSD test. The p value was considered significant as the following: $p > 0.05$: non-significant, $p < 0.05$: significant and $p < 0.001$: highly significant.

.

## Results

### *Gross observation*

GI showed no gross changes, no hair loss, no skin ulcerations, normal pale pink color of the HBP with neither pathological nor inflammatory changes. Their buccal pouch lengths were about 5- 5.5 cm for all hamsters **(Fig. 3A)**. GII showed marked hair loss, pouch depth shrinkage, skin ulcers and marked debilitation of all animals. Animal pouches showed large exophytic growths with pronounced vascularity and the pouch length ranged from 1.5-2cm in addition to eroded and ulcerative areas with spontaneous bleeding were seen **(Fig. 3B)**. The mean tumors volume measurement of tumor-bearing animals in ten hamsters in GII was 768.4 mm3 (737.7 – 799.1 mm3). GIII and GIV showed slight improvement in the general health. The length of the pouches was about 2- 2.5cm. Slight decrease in size of the papillomatous lesions was observed compared to GII **(Fig. 3C&D)**. The mean tumors volume measurement in those of GIII and GIV was 443.1 mm3 (422.4 – 463.8 mm3) and 422.3 mm3 (390.2 – 454.4 mm3), respectively. GV showed marked improvement in general health of the animals. There was a significant increase of the pouch length to about 3.5 - 4cm. The mean tumors volume measurement in those of GV was 30.2 mm3 (25.9 – 34.5 mm3). There was highly significant difference (p value < 0.001) of tumor volume in GIII, GIV or GV, comparing to GII. There was marked decrease in the size of exophytic masses in GV when compared to animals treated in GII, GIII, GIV or GV **(Fig. 3E)**, **(Table. 1)**

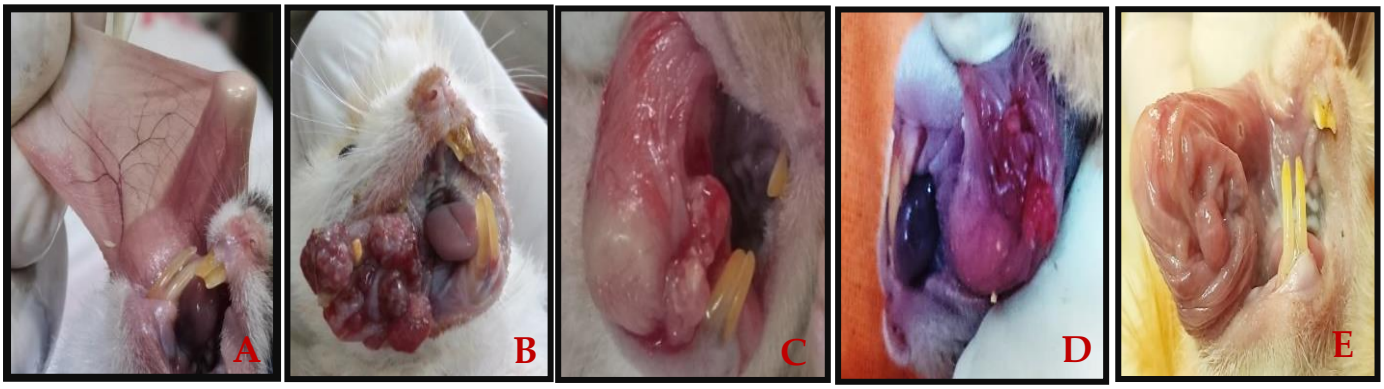


**(Fig. 3A):** Photograph of GI showing normal buccal pouch mucosa which appeared pink in color with smooth surface. **(Fig. 3B):** Photograph of GII showing multiple exophytic papillary tumor masses surrounded with bleeding areas. **(Fig. 3C):** Photograph of GIII showing small tiny elevation with an absence of ulceration and bleeding. **(Fig. 3D):** Photograph of GIV showing small size nodule with an absence of ulceration and bleeding. **(Fig. 3E):** Photograph of GV showing small size of tumor masses with an absence of ulceration and bleeding.

**Table 1: Common clinical findings observed in the studied groups.**

| Features | Groups | | | | |
|---|---|---|---|---|---|
| | GI | GII | GIII | GIV | GV |
| Loss of appetite | - | +++ | ++ | ++ | + |
| Inactivity | - | +++ | ++ | ++ | + |
| Corner huddling | - | +++ | ++ | ++ | + |
| Sneezing, wheezing, and/or discharge from the nose or eyes, | - | +++ | ++ | ++ | + |
| Wetness around the tail, diarrhea | - | +++ | ++ | ++ | + |
| Hair loss | - | +++ | ++ | ++ | + |
| **Gross observations** | | | | | |
| Papillomatous lesion | - | +++ | ++ | ++ | + |
| Pouch length | 5 cm | 1.5-2cm | 2.5-3.5cm | 2.5-3.5cm | 3.5-4.5cm |
| Ulcers | - | +++ | ++ | ++ | + |
| Exudation | - | +++ | ++ | ++ | + |
| Tumors | - | 100 % | 50 % | 50 % | 30% |

– = no change; + = mild; ++ = moderate; +++ = severe

*Histological findings*

**GI** revealed normal thin stratified squamous epithelium, sub-epithelial connective tissue (C.T) and muscular layer were seen **(Fig.4A)**. **GII** revealed large papillomatous lesions in the overlying epithelium with different degrees of epithelial dysplasia with true invasion of well to moderate differentiated SCC with invading islands of epithelium into underlying C.T (DOI=10.7mm) **(Fig.2)**. The invading epithelial cells showed hyperchromatism, prominent nucleoli, altered N\C ratio, swirling of spinous layer and cellular and nuclear pleomorphism with marked chronic inflammatory cells. **(Fig.4B)**. **GIII** and **GIV** revealed moderate to severe epithelial dysplasia with areas of top to bottom changes or carcinoma in situ (CIS)were seen in five hamsters while the other five hamsters showed superficial invasion of malignant cells in the form of well differentiated SCC which was limited to the nodules only, not extended to deeper areas (DOI=1.7-1.9mm). There was reduction of the distal necrosis, inflammatory infiltration and increase amount of collagen fibers (**Fig.4C&D)**. GV revealed moderate to severe epithelial dysplasia were seen in seven hamsters (epithelium had focal areas of dysplasia represented as hyperchromatism, altered N/C ratio; cellular and nuclear pleomorphism, prominent nucleoli, as well as multiple group cell keratinization while the other three hamsters showed well differentiated SCC which was juxta-epithelial and not extended to the deeper C.T (DOI=0.8mm) with increased amount of keratin formation. The C.T showed almost decrease of eroded areas, inflammatory infiltration and increase thickness of striated muscle layer and the tumor masses were mostly replaced by proliferated fibrous tissue with more collagen deposition **(Fig.4E).**

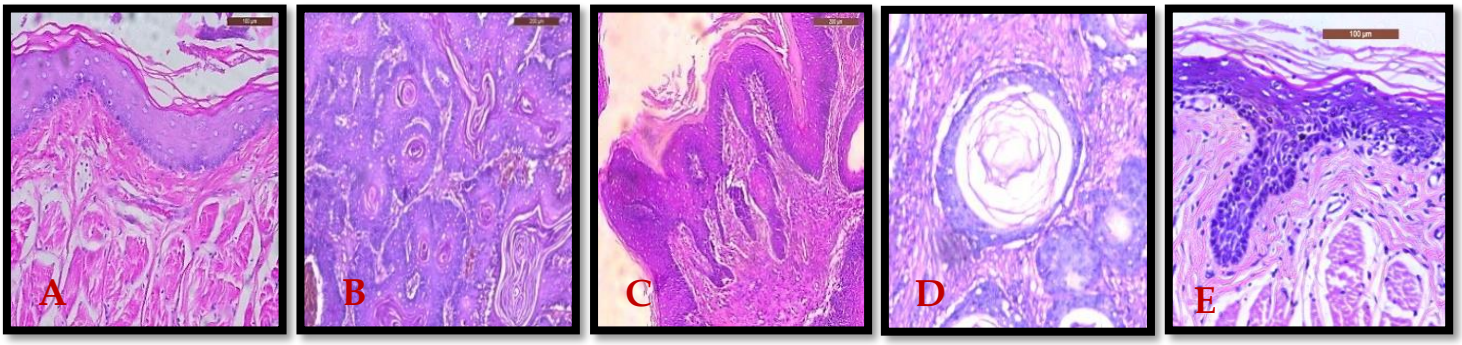


**(Fig.4A):** Photomicrograph of GI showing: stratified squamous epithelium exhibiting keratinization, flattened rete ridges, C.T layer, muscular layer and deep layer of loose areolar connective tissue (H&E stain X200). **(Fig.4B):** Photomicrograph of GII showing well differentiated SCC with deep invasion of multiple tumor islands into the underlying connective tissue and sub-epithelial inflammatory infiltrates (H&E stain X100). **(Fig.4C):** Photomicrograph of GIII showing well differentiated SCC (superficial invasion) (H&E stain X200). **(Fig.4D):** Photomicrograph of GIV showing well differentiated SCC (nests and pearls) (H&E stain X200). **(Fig.4E):** Photomicrograph of GV showing severe dysplasia (H&E stain X200).

*Immunohistochemical findings:*

BMI-1 staining exhibited positive nuclear expression throughout the epithelial layers and invading tumor cells **(Fig. 5A-E)**.GI recorded the lowest mean area percentage (10.2 %), while GII had the highest mean area percentage (75.3 %). Comparing the various treated groups (GIII, GIV and GV), GV showed highly significant difference (p value < 0.001) with either GIII or GIV. There was non-significant difference (p value = 0.125) between GIII and GIV. Comparing the positive control group (GII) with the various treated groups (GIII, GIV, and GV), there was highly significant difference (p value < 0.001) between (GII and GIII), (GII and GIV) and (GII and GV). Comparing the control groups (GI and GII), there was highly significant difference (p value < 0.001) between GI& GII **(Table.2 & Fig.6).**

VEGF staining exhibited positive cytoplasmic expression throughout the epithelial layers and invading tumor cells **(Fig. 5F-J)**. GI recorded the lowest mean area percentage (19.70 %), while GII had the highest mean area percentage (70.20 %). Comparing the various treated groups (GIII, GIV and GV), GV showed highly significant difference (p value < 0.001) with either GIII or GIV. There was highly significant difference (p value < 0.001) between GIII and GIV. Comparing the positive control group (GII) with the various treated groups (GIII, GIV, and GV), there was highly significant difference (p value < 0.001) between GII and GV. Comparing the control groups (GI and GII), there was highly significant difference (p value < 0.001) between GI and GII **(Table.3 & Fig.6)**.

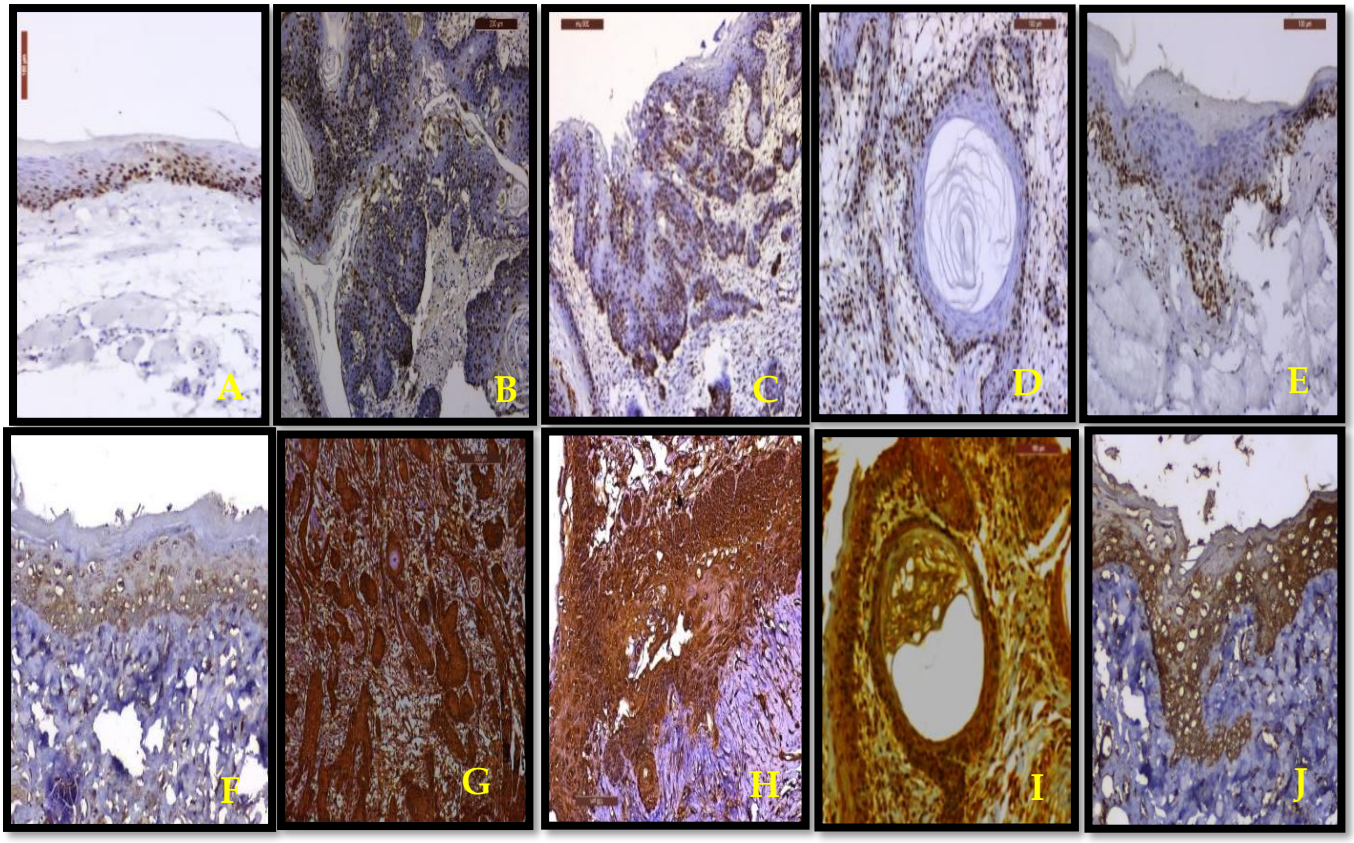


**Fig.5A-D):** Photomicrograph representative images of the expression of **BMI-1** between all groups from GI to GV respectively. (Streptavidin biotin peroxidase). **(Fig.5F-J):** Photomicrograph representative images of expression of **VEGF** between all groups from GI to GV respectively. (Streptavidin biotin peroxidase).

**Table (2): Comparison between the studied groups regarding BMI-1 level**

| | BMI-1 | | P-value for post analysis using LSD test | | | | |
|---|---|---|---|---|---|---|---|
| | Mean ± SD | Range | G1 | GII | GIII | GIV | GV |
| Group I | 10.20 ± 1.87 | 7.2 – 13.2 | -- | 0.000 | 0.000 | 0.000 | 0.000 |
| Group II | 75.30 ± 2.45 | 71.3 – 79.3 | 0.000 | -- | 0.000 | 0.000 | 0.000 |
| Group III | 52.10 ± 2.28 | 48.9 – 55.3 | 0.000 | 0.000 | -- | 0.125 | 0.000 |
| Group IV | 50.30 ± 2.54 | 46.4 – 54.2 | 0.000 | 0.000 | 0.125 | -- | 0.000 |
| Group V | 32.60 ± 3.47 | 27.9 – 37.3 | 0.000 | 0.000 | 0.000 | 0.000 | -- |
| **F** | **888.742** | | | | | | |
| **P-value** | **<0.001 (HS)** | | | | | | |

**Table (3): Comparison between the studied groups regarding VEGF level**

| | VEGF | | P-value for post analysis using LSD test | | | | |
|---|---|---|---|---|---|---|---|
| | Mean ± SD | Range | G1 | GII | GIII | GIV | GV |
| Group I | 19.70 ± 3.40 | 15.1 – 24.3 | -- | 0.000 | 0.000 | 0.000 | 0.000 |
| Group II | 70.20 ± 3.72 | 65.3 – 75.1 | 0.000 | -- | 0.000 | 0.000 | 0.000 |
| Group III | 51.80 ± 4.00 | 46.9 – 56.7 | 0.000 | 0.000 | -- | 0.000 | 0.000 |
| Group IV | 42.40 ± 4.19 | 36.9 – 47.9 | 0.000 | 0.000 | 0.000 | -- | 0.000 |
| Group V | 26.80 ± 2.89 | 22.8 – 30.8 | 0.000 | 0.000 | 0.000 | 0.000 | -- |
| **F** | **300.392** | | | | | | |
| **P-value** | **<0.001 (HS)** | | | | | | |

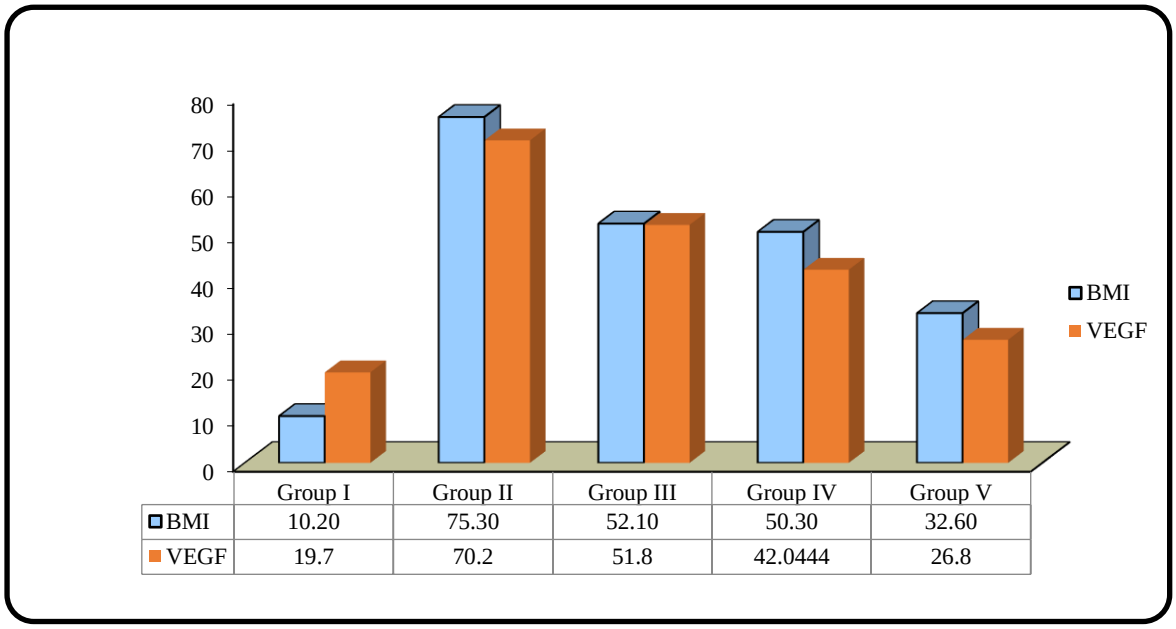


**Fig.(6):** Comparison between the studied groups regarding BMI-1 and VEGF levels.

*Correlation analysis*

There was a statistically significant difference (p value < 0.001) positive (direct) correlation between area % of BMI-1 and area % of VEGF (**(Table. 4**, **Fig.**7**)** or between tumor volume and area % of BMI-1 & VEGF expressions (p value < 0.001) **(Table. 4 Fig.**8**).** This means that an increase in one variable is associated with an increase in the other variable and vice versa.

**Table (4):** Correlation between area % of BMI-1and area % of VEGF and between tumor volume and area % of BMI-1 & VEGF in all the studied groups.

| | Correlation coefficient (r) | p-value |
|---|---|---|
| **BMI-1 vs VEGF** | **0.923** | **0.000** |
| **Tumor volume vs area % of BMI-1** | **0.850** | **0.000** |
| **Tumor volume vs area % of VEGF** | **0.907** | **0.000** |

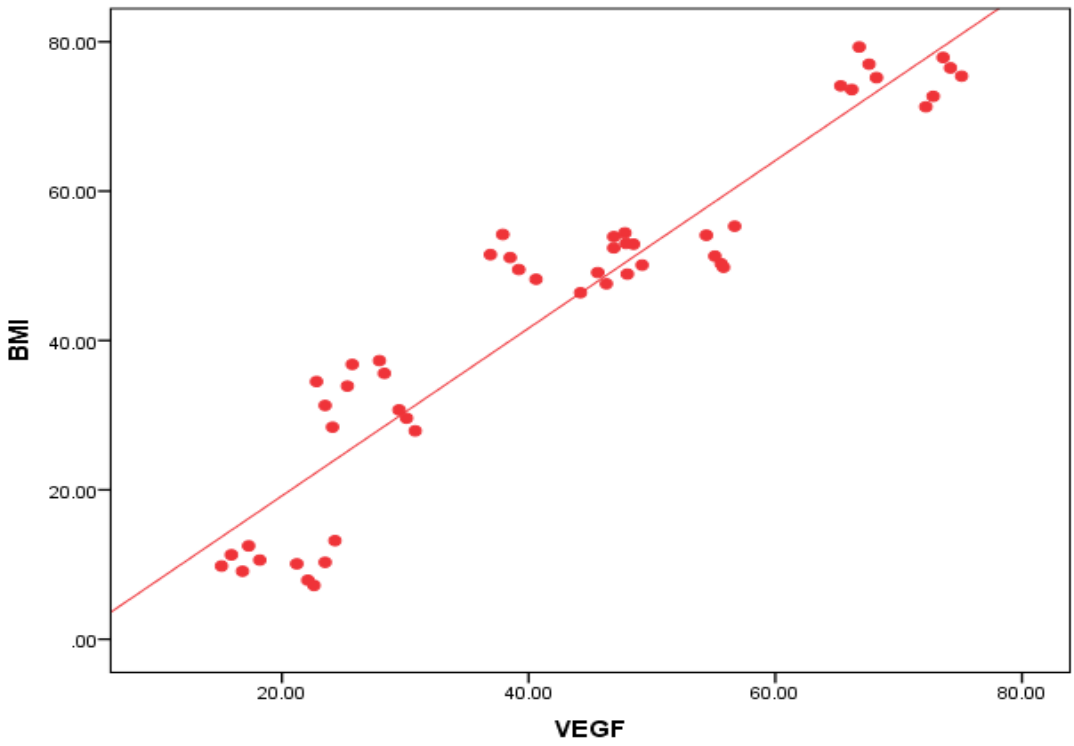


**Fig. (7):** Correlation between area % of BMI-1 and area % of VEGF expressions.

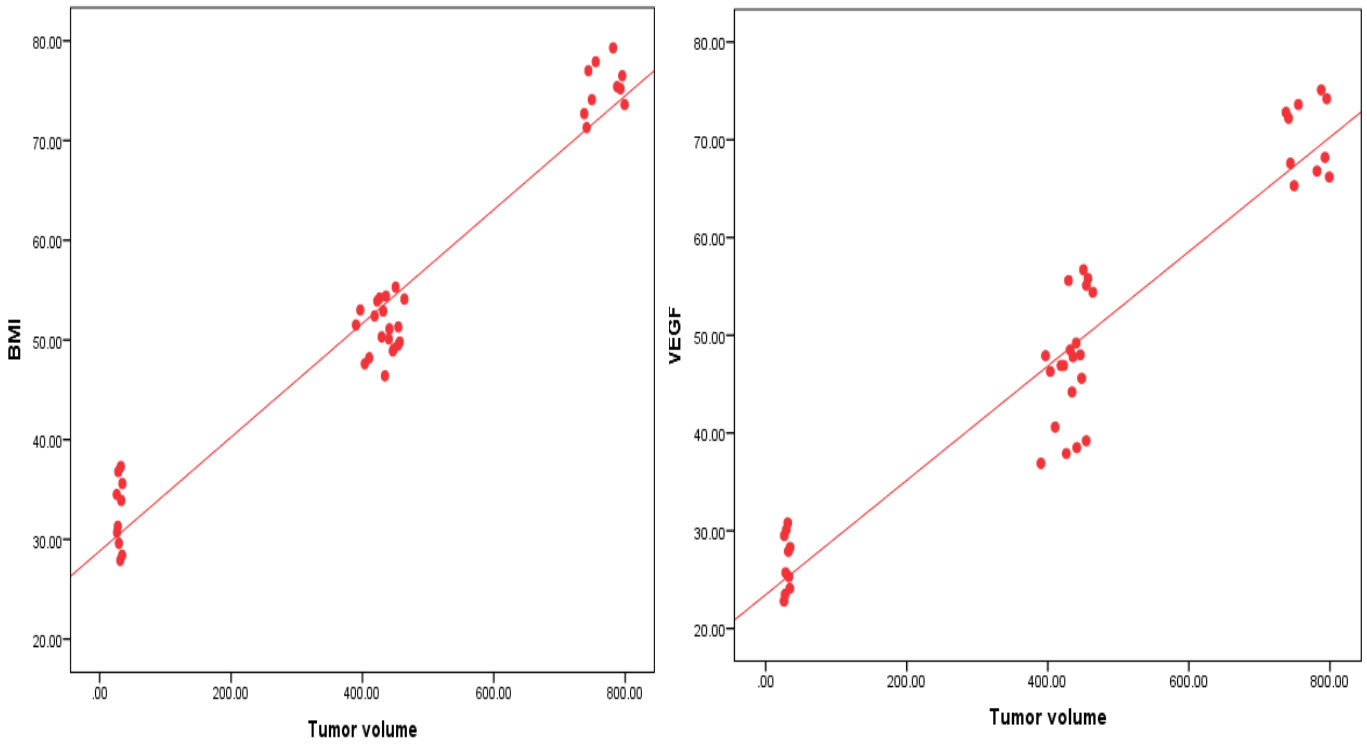


**Fig. (8):** Correlation of tumor volume and area % of BMI-1 and VEGF expressions.

## Discussion

Oral cancer considers as one of the most common cancers worldwide. Despite easy access to the oral cavity and significant advances in treatment, the morbidity and mortality rates for oral cancer patients are still very high. The model of hamster cheek pouch system of oral carcinoma is useful and important in deeper understanding of cancer biology, diagnosis and treatment modalities. In the current work the results of general health observations, tumor volume, H&E stain, DOI, IHC staining utilizing BMI-1 and VEGF antibodies showed variable insights.

In the present study, the gross observation findings in GI (normal group) showed no observable abnormalities of the HBP with normal histological structures. These results are in agreement with the studies reported the same findings(3, 5, 7). This finding reflected on H&E staining which showed normal thin stratified squamous epithelium formed of two to four cell layers, lacking rete ridges and thin keratin surface layer. The underlying CT showed non inflamed loose connective tissue, with thin vascular spaces. This result is in agreement with that of other investigators(2, 4, 8).

In the current study, GII showed marked perioral hair loss, pouch depth shrinkage, skin ulcers and marked debilitation of all animals. Animals' pouches showed large exophytic growths with pronounced vascularity and the pouch length (1.5-2cm) which was decreased compared to GI **(**5- 5.5 cm **)**due to necrosis in the distal end of the pouch. These observations are mainly due to the strong toxic DMBA effect(7). By using H&E stain, a development of various patterns of invasive SCC (50% well differentiated and 50% moderately differentiated) were seen which extended to deeper areas of C.T (DOI=10.9 mm). This is in consistence with that shown by other researchers(2-7). In agreement with the results of the present work, Balakrishnan et al (2022)(6), found that 100% tumor formation after 14 weeks of painting DMBA alone on the hamster cheek pouches. These results did not differ much from other studies done by Manimaran et al(2017)(9), and Selvasundaram et al(2018)(10). This may be attributed to procarcinogenic nature of DMBA, which metabolized by phase I enzymes such as cytochrome P450 to its ultimate carcinogenic metabolite, dihydrodiol epoxide, which binds to and damage DNA, contributing to mutation and carcinogenesis. And also, ROS has been implicated in all the three stages (initiation, promotion, and progression) of carcinogenesis. ROS-mediated DNA damage could cause structural modifications in DNA, activation of proto-

oncogene, and inactivation of tumor suppressor genes, which eventually leads to neoplastic transformation.

In the present study, GIII showed a relatively slight improvement in the animal general health. The pouch length was increased (2.5-3.5cm) compared to GII (1.5-2cm) due to reduction of the inflammatory infiltration. A relatively shrinkage in size of the papillomatous lesions was observed. These findings conflicted on H&E staining in which five hamsters revealed different degrees of epithelial dysplasia (moderate (10%), severe (20%) or CIS (20%) while the other five hamsters showed superficial invasion of well differentiated SCC (50 %), not extended to deeper areas (DOI=1.9mm). This is in line with other studies(49, 59). Topically applied imiquimod inhibited tumor growth. This effect was associated with increased tumor infiltration by DC and T cells and was abolished by depletion of CD8+ cells(50). Vola et al (2018)(55) described that, tumor-specific CD8+ T cells were increased in imiquimod-treated mice, and local tumor control was associated with decreased spontaneous lung metastases, an effect that could result from decreased seeding from the treated tumor and/or inhibition by antitumor T cells that are active systemically. However, evidence by Patinote et al (2020)(60), indicates that the antitumor effect of topical imiquimod, at least within the first 1 or 2 weeks, can be entirely mediated by plasmacytoid dendritic cells (pDCs) that acquire CD8 and lytic function. Mane et al (2021)(62), Wester et al (2017)(61) also showed elevated levels of monocyte chemotactic protein1/CCL2 and IL-21 in the tumor microenvironment following imiquimod application. Monocyte chemotactic protein1/ CCL2 may contribute to pDC recruitment, whereas IL-21 has been shown to be implicated in triggering pDC degranulation, increasing the potential of cytotoxic effector T and NK cells and hampering Treg expansion. Fujimura et al (2018)(54) found that, CCL17 and CCL22 from TAMs attracts Tregs to the tumor site by immunomodulatory reagents imiquimod are useful for suppressing tumor growth.

In the present study, GIV showed almost the same clinical and histological results as GIII. This is in line with other antiangiogenic studies(32, 40). Tamura et al (2016)(33), stated that, bevacizumab demonstrated characteristic histological changes such as disappearance of microvascular proliferation and significant reduction of microvessel density, suggesting the normalization of the vascular structure. Yoshida et al (2018)(31), found that, bevacizumab injections were identified to inhibit tumor growth in OSCC xenografts. It was also demonstrated that treatment with bevacizumab significantly reduced the microvessel densities and increased the tumor apoptosis index. Erlotinib (small-molecule tyrosine kinase inhibitors) demonstrated modest improvements when used in combination with bevacizumab in recurrent/metastatic OSCC(31, 41).

In the present study, GV as a combination group showed marked improvement in animal general health compared to imiquimod G or bevacizumab G alone. There was a marked increase of the pouch length (3.5 - 4.5cm) due to the observable decrease of eroded areas and inflammatory infiltration. Also, there was marked decrease in the size of exophytic masses in GV when compared to the animals treated with imiquimod or bevacizumab only. These findings conflicted on H&E staining which revealed different degrees of epithelial dysplasia mild (10%), moderate (30%), severe (20%) or CIS (10%), in addition to well differentiated SCC (30%) which was juxta-epithelial and not extended to the deeper C.T (DOI=0.9mm) with increased amount of keratin formation. The CT showed marked increase thickness of striated muscle layer and the tumor masses were mostly replaced by proliferated fibrous tissue with more collagen deposition. These findings reflected the beneficial effect of combining imiquimod with bevacizumab in order to achieve these positive results. Imiquimod may contribute to antitumor responses by affecting tumor cells, tumor-infiltrating immune cells, and the tumor microenvironment. This broad range of antitumor activities make imiquimod a good candidate for use as adjuvant combined with other therapies, particularly to enhance immunotherapy. Chen et al(2018)(42) demonstrated that the combination of bevacizumab with immunotherapy causes a synergistic inhibition of tumor growth and metastases in human cancers. Vidovic et al (2021)(56) found that combining imiquimod with intra-lesional IL-2, largely inhibited the growth of tumor cells, and enhanced the efficacy of imiquimod.

In the current study, IHC staining of GI showed positive nuclear expression of BMI-1 (10.2 %) that was seen to be restricted to the basal and supra-basal epithelial layers and almost negative in the remaining epithelial cell layers. This result is in agreement with that of other investigators(17, 20). Kalish et al (2020)(20) stated that, BMI-1 was found to be necessary for the self-renewal of both normal and cancer stem cells. Yet, the stemness genes regulated by BMI-1 remain unknown. Thus, understanding the molecular mechanisms by which BMI-1 regulates the stem cell properties is likely to pave the way for newer therapeutic modules.

In the current study, IHC staining of GII showed positive nuclear expression of BMI-1 (75.30 %) that was seen throughout the epithelial layers and invading tumor cells, that showed highly significantly expression compared to GI ($p$ value < 0.001). This result is in agreement with that of other investigator(21). Several studies have reported that BMI-1 was overexpressed in OSCC cells

when correlated to normal epithelium and was thought to impact cell proliferation and survival in OSCC(19, 22). Curtarelli et al (2018)(16) added that the expression of BMI-1 was correlated with poor overall survival and was also associated with lymph node metastasis and clinical stage.

Association of BMI-1 overexpression, and stem-like properties in tumor cells could be attributed to induction of the EMT that promoted invasion, metastasis, and poor prognosis(22). In the same background, Herzog et al (2021)(23) showed that BMI-1 was necessary for EMT during tumor development in head and neck carcinomas particularly OSCC patients. Strong evidence suggested that BMI-1 was important to invasive potential and favored to the maintenance and self-renewal of CSCs in several tumor types, including OSCC(23). As a stem cell marker, BMI-1 played a key role in the functioning of endogenous stem cells and CSCs(18). Patel et al (2018)(25) indicated that silencing BMI-1 can inhibit the malignant biological behavior of cancer, in addition to the self-renewal and differentiation of CSCs.

In the present study, IHC staining of GIII showed positive nuclear expression of BMI-1 (52.10 %) that was seen throughout the epithelial layers and invading tumor cells, that showed highly significant difference (p value < 0.001) compared to GII. This result is in agreement with that shown by Ren et al (2016)(51) whom found that, TLR7 agonist imiquimod was able to suppress HCC stem cell proliferation and self-renewal, an effect which may be mediated by TLR7-IKK-NFκB-IL6 signaling.

In the present study, IHC staining of GIV showed positive nuclear expression of BMI-1 (50.30 %) that was seen throughout the epithelial layers and invading tumor cells, that showed highly significant difference (p value < 0.001) compared to GII. This result is in agreement with that of other investigators(20, 24). In glioblastoma, the VEGF tyrosine kinase inhibitor-bevacizumab has proven successful in expanding survival time by targeting the perivascular niche. Also in glioblastoma, the VEGF-VEGF2-NRP1 axis is seen as an attractive target in order to decrease CD133+glioblastoma CSCs(47).

In the current study, IHC staining of GV showed positive nuclear - cytoplasmic expression of BMI-1 (32.60 %) that was seen throughout the epithelial layers and invading tumor cells, that showed highly significant difference (p value < 0.001) compared to GII as well as to either GIII or GIV. This is in line with that shown by Zhao et al (2013)(26) whom found that, Bevacizumab combined with anti-hepatoma-derived growth factor (HDGF) antibody has been shown to suppress CSC populations in NSCLC.

In the current study of GI showed positive cytoplasmic expression of VEGF (19.7 %) that was seen in almost all normal epithelial cells as membranous staining, which was predominantly detected in the basal layer. This result is in agreement with that of other investigators(35). It is evident that VEGF has a role in the embryonic angiogenesis and in physiological angiogenesis processes, such as corpus luteum development and wound healing. VEGF is expressed in embryo and many human and mouse adult organs, including lung, kidney, adrenal gland, and heart. VEGF is also detected in the cultured human primary keratinocytes and the saliva of healthy individuals(39).

In the current study, IHC staining of GII showed positive cytoplasmic expression of VEGF (70.20 %) that was seen throughout the epithelial layers and invading tumor cells, that showed highly significant (p value < 0.001) expression compared to GI. This result is in agreement with that of other investigator(34, 35). Martano et al (2016)(36) identified marked increase in VEGF expression during the transition between normal and OSCC tissues, in association with an increasing grade of differentiation. This was indicated by a high number of VEGF-positive cells associated with the accumulation and consequent loss of cytoplasmic polarization of VEGF granules in less differentiated tumors. Siva Shankari et al (2018)(37), indicated a significant upregulation of VEGF expression during the transition from normal oral epithelium through dysplasia to invasive OSCC, but no correlation was found between VEGF expression and the grade of dysplasia, while Araki-Maeda et al (2022)(38), found a correlation between VEGF and the different degrees of oral dysplasia and carcinoma.

In the current study, IHC staining of GIII showed positive cytoplasmic expression of VEGF (51.80 %) that was seen throughout the epithelial layers and invading tumor cells, that showed highly significant (p value < 0.001) expression compared to GII. This result is in agreement with that of other investigators(52, 57). Aspord et al (2014)(57) revealed that, tumor cells secrete many potent angiogenic factors such as VEGF, fibroblast growth factor, angiogenin, and IL-8, which drive angiogenesis, critical for tumor growth and invasiveness. Tumor cell elimination may thus directly reduce the level of tumor derived factors, especially proangiogenic factors. The large amounts of IFN-a and IP10 produced by pDCs in response to imiquimod stimulation are described to be antiangiogenic and can downregulate VEGF and fibroblast growth factor production(58). Wu et al (2020)(53) found that the antiangiogenic effect of topical imiquimod is mediated by several cytokines, including IFNγ, TNFα and IL-18.

In the current study, IHC staining of GIV showed positive cytoplasmic expression of VEGF (42.40 %) that was seen throughout the epithelial layers and invading

tumor cells, that showed highly significant (p value < 0.001) expression compared to GII. This result is in agreement with that of other investigators(43). Yadav et al (2021)(43), observed decreased expression of VEGF after bevacizumab treatment which binds to and neutralizes VEGF proving that bevacizumab exert anti-angiogenic effects through inactivation of the VEGF receptor on tumor cells.

In the present study, IHC staining of GV showed positive cytoplasmic expression of VEGF (26.80 %) that was seen throughout the epithelial layers and invading tumor cells, that showed highly significant difference (p value < 0.001) compared to GII as well as to either GIII or GIV. This is in line with that shown by Damiano et al(2007)(44) whom concluded that, the combination of TLR agonist and bevacizumab cooperates in reducing the levels of hVEGF but not mVEGF. Their results suggest that the murine-dependent immune-mediated effects of TLR agonist enhance the activity of bevacizumab on the tumor cells.

They demonstrated that TLR agonist inhibits proliferation, adhesion, and migration of endothelial cells and, importantly, the VEGF-stimulated capillary tube and network formation. Therefore, it is likely that the well documented inhibitory effect of bevacizumab on vessel formation, due to VEGF inhibition, combined with the interference of TLR agonist on critical functions of tumor endothelial cells, may finally be responsible for the cooperative effect observed. The rationale for combining anti-angiogenics with immunotherapy is based on the immunosuppressive properties of VEGF, which has been shown to decrease T cell recruitment and infiltration into the tumor, reduce adhesion of immune effector cells to tumor vessels, hampers T cell function, affects the functional capacity of dendritic cells and enables the accumulation of Tregs(48).

In the present study, there was a statistically significant positive (direct) correlation either between BMI-1 and VEGF (p value > 0.001) or between tumor volume and area % of BMI-1 & VEGF expressions (p value > 0.001). This means that an increase in one variable is associated with an increase in the other variable and vice versa. Wang et al (2015)(27) have revealed the involvement of the BMI-1/NF-κB/VEGF signaling pathway in the promotion of glioma cell-mediated migration of endothelial cells and neovascularization in vitro and in vivo, while NF-κB inhibition was demonstrated to reverse these effects.

These results demonstrated that BMI-1 is involved in the invasiveness of cancer by regulating the expression of PTEN and the vascular endothelial growth factor(29). Li et al (2013)(28) found that, Bmi-1 knockdown decreased the expression and activities of MMP-2, MMP-9 and VEGF. These results suggest that Bmi-1 knockdown inhibits HCC cell invasion by suppression of MMP-2, MMP-9 and VEGF. Meng et al (2012)(30) demonstrated that knockdown of B-1 inhibits lung adenocarcinoma cell migration and metastasis by diminishing VEGF secretion via the PTEN/PI3K/Akt signaling pathway.

## Conclusion

This study realized that CSCs can enhance tumor progression either by CSCs immunoediting that can survive in immunocompetent host or by establishing conditions that facilitate neoplastic growth within the tumor microenvironment. our results demonstrated that combination of imiquimod-bevacizumab has an inhibitory effect on tumor progression in OSCC, which was found to be more efficient than either agent alone. Regarding efficacy, a (10 mg/ml) of bevacizumab once daily for a week combined with 5% imiquimod once daily for 4 weeks afford a prominent response rate, which was evident in terms of gross observation, tumor volume, histopathological examination, DOI, IHC staining of BMI-1 and VEGF. Therefore, specific targeting of CSCs by immunotherapeutic approaches may lead to more efficient and lasting therapeutic results in the future. Accordingly, Further studies to be carried out on the same model, with increase concentration or dose of the used drugs and/or change the way of administration.

**Funding:** This research did not receive any specific grant from funding agencies in the public, commercial, or not-for-profit sectors.

**Institutional Review Board Statement:** The National Research Council Guide for the care and use of laboratory animals have been followed. All experiments were approved by ethical committee of Faculty of Dental Medicine, Al-Azhar University, Egypt (Ethical Code No. 148/164, 30-04-2019).

**Informed Consent Statement:** Not applicable.

**Data Availability Statement:** The data sets used during current study are available from the corresponding author on reasonable request.

**Conflicts of Interest:** The authors declare no conflict of interest.

## References

1. Sung H, Ferlay J, Siegel R, Laversanne M, Soerjomataram I, Jemal A, et al. Global cancer statistics 2020: GLOBOCAN estimates of incidence and mortality worldwide for 36 cancers in 185 countries. CA Cancer J Clin. 2021;71(3):209-49.
2. Shamia A, Abd-Alhafez A, Al-qalshy E, Zouair M. Therapeutic efficacy of time-dependent cetuximab on experimentally induced hamster buccal pouch carcinoma. Int J Health Sci. 2022;6(S5):3431-3456.
3. Saleh M, Darwish Z, El Nouaem M, Mourad G, Ramadan O. Chemopreventive effect of green tea and curcumin in induced oral squamous cell carcinoma: an experimental study. Alex Dent J. 2020;45(3):74-80.
4. Martínez B, Gómez P, Castro C, Pérez J. DMBA-induced oral carcinoma in Syrian hamster: Increased carcinogenic effect by dexamethasone coexposition. Biomed Res Int. 2020;1-8.
5. Nagini S, Kowshik J. The hamster buccal pouch model of oral carcinogenesis. Methods Mol Biol. 2016;1422:341-50.
6. Balakrishnan V, Ganapathy S, Veerasamy V, Duraisamy R, Sathiavakoo V, Krishnamoorthy V, et al. Anticancer and antioxidant profiling effects of Nerolidol against DMBA induced oral experimental carcinogenesis. J Biochem Mol Toxicol. 2022;36(6):e23029.
7. El-Hossary W, Hegazy E, El-Mansy M. topical chemopreventive effect of thymoquinone versus thymoquinone loaded on gold nanoparticles on dmba-induced hamster buccal pouch carcinogenesis (immunohistochemical study). Egypt Dent J. 2018;64(4):3523-33.
8. Ezzat S, AbuElkhair M, Mourad M, Helal M, Grawish M. Effects of aqueous cinnamon extract on chemically-induced carcinoma of hamster cheek pouch mucosa. Biochem Biophys Rep. 2017; 12: 72–78.
9. Manimaran A, Buddhan R, Manoharan S. Emodin downregulates cell proliferation markers during DMBA induced oral carcinogenesis in golden Syrian hamsters. Afr J Tradit Complement Altern Med. 2017 ;14(2):83-91.
10. Selvasundaram R, Manoharan S, Buddhan R, Neelakandan M, Murali-Naidu R. Chemopreventive potential of esculetin in 7, 12-dimethylbenz (a) anthracene-induced hamster buccal pouch carcinogenesis. Mol Cell Biochem. 2018 Nov;448(1-2):145-153.
11. Hussein A, El-Sheikh S, Darwish Z, Hussein K, Gaafar A. Effect of genistein and oxaliplatin on cancer stem cells in oral squamous cell carcinoma: an experimental study. Alex Dent J. 2018;43(1):117-23.
12. Yang Y, Zhou Z, Ge J. Effect of genistein on DMBA-induced oral carcinogenesis in hamster. Carcinogenesis 2006;27(3):578-83.
13. Li N, Chen X, Liao J, Yang G, Wang S, Josephson Y, et al. Inhibition of 7, 12-dimethylbenz [a] anthracene (DMBA)-induced oral carcinogenesis in hamsters by tea and curcumin. Carcinogenesis 2002;23(8):1307-1
14. Al-Dosoki M, Abd-Alhafez A, Omar A, Zouair M. Flow cytometric assessment of nivolumab and/or epigallocatechin-3-gallate oncancer stem cells of DMBA induced hamster buccal pouch carcinoma.. Med Sci. 2021;25(118):3206-21.
15. Simple M, Suresh A, Das D, Kuriakose M. Cancer stem cells and field cancerization of oral squamous cell carcinoma. Oral Oncol. 2015;51(7):643-51.
16. Curtarelli R, Gonçalves J, Dos-Santos L, Savi M, Nör J, Mezzomo L, et al. Expression of cancer stem cell biomarkers in human head and neck carcinomas: a systematic review. Stem cell reviews and reports 2018;14(6):769-84.
17. Wu T, Li Y, Ma S, Bing-Liu, Zhang W, Sun Z. Expression and associations of TRAF1, BMI-1, ALDH1, and Lin28B in oral squamous cell carcinoma. Tumour Biol. 2017;39(4):1010428317695930.
18. Zhou M, Xu Q, Huang D, Luo L. Regulation of gene transcription of B lymphoma Mo-MLV insertion region 1 homolog. Biomed Rep. 2021;14(6):52.
19. Zhao T, Liang S, Ju W, Liu Y, Tan Y, Zhu D, et al. Normal BMI predicts the survival benefits of inductive docetaxel, cisplatin, and 5-fluorouracil in patients with locally advanced oral squamous cell carcinoma. Clin Nutr. 2020 Sep;39(9):2751-58.
20. Kalish J, Tang X, Scognamiglio T, Zhang T, Gudas L. Doxycycline-induced exogenous Bmi-1 expression enhances tumor formation in a murine model of oral squamous cell carcinoma. Cancer Biol Ther. 2020;21(5):400-411.
21. Kurihara K, Isobe T, Yamamoto G, Tanaka Y, Katakura A, Tachikawa T. Expression of BMI1 and ZEB1 in epithelial-mesenchymal transition of tongue squamous cell carcinoma. Oncol Rep. 2015;34(2):771-78.
22. Chou C, Yang N, Liu T, Tai S, Hsu D, Chen Y, et al. Chromosome Instability Modulated by BMI1–AURKA Signaling Drives Progression in Head and Neck CancerBM11-AURKA Axis in Cancer Progression. Cancer Res. 2013;73(2):953-66.
23. Herzog A, Warner K, Zhang Z, Bellile E, Bhagat M, Castilho R, et al. The IL-6R and Bmi-1 axis controls self-renewal and chemoresistance of head and neck cancer stem cells. Cell Death Dis. 2021;12(11):988.
24. Klein I, Meurer L, Danilevicz C, Squarize C, Martins M, Carrard V. BMI-1 expression increases in oral leukoplakias and correlates with cell proliferation. J Appl Oral Sci. 2020;28:e20190532.
25. Patel N, Garikapati K, Makani V, Nair AD, Vangara N, Bhadra U, et al. Regulating BMI1 expression via miRNAs promote Mesenchymal to Epithelial Transition (MET) and sensitizes breast cancer cell to chemotherapeutic drug. PLoS One. 2018;13(2):e0190245.
26. Zhao J, Ma M, Ren H, Liu Z, Edelman M, Pan H, et al. Anti-HDGF Targets Cancer and Cancer Stromal Stem Cells Resistant to ChemotherapyTargeting HDGF to

Inhibit Cancer Stem Cells. Clin Cancer Res. 2013;19(13):3567-76.
27. Wang M, Li C, Cui J, Jiao M, Wu T, Jing L, et al. BMI-1, a promising therapeutic target for human cancer. Oncol Lett. 2015;10(2):583-88.
28. Li X, Yang Z, Song W, Zhou L, Li Q, Tao K,et al. Overexpression of Bmi-1 contributes to the invasion and metastasis of hepatocellular carcinoma by increasing the expression of matrix metalloproteinase (MMP)-2, MMP-9 and vascular endothelial growth factor via the PTEN/PI3K/Akt pathway. Int J Oncol. 2013;43(3):793-802.
29. Vlachostergios P, Papandreou C. The Bmi-1/NF-κB/VEGF story: another hint for proteasome involvement in glioma angiogenesis?. J Cell Commun Signal. 2013;7(4):235-37.
30. Meng X, Wang Y, Zheng X, Liu C, Su B, Nie H, et al. shRNA-mediated knockdown of Bmi-1 inhibit lung adenocarcinoma cell migration and metastasis. Lung Cancer 2012;77(1):24-30.
31. Yoshida H, Yoshimura H, Matsuda S, Ryoke T, Kiyoshima T, Kobayashi M, et al. Effects of peritumoral bevacizumab injection against oral squamous cell carcinoma in a nude mouse xenograft model: A preliminary study. Oncol Lett. 2018;15(6):8627-34.
32. Juanes C, Souza S, Braga V, Barreto F, Aguiar G, Pimentel K, et al. Red propolis and L-lysine on angiogenesis and tumor growth in a new model of hamster cheek pouch inoculated with Walker 256 tumor cells. Einstein (São Paulo) 2019;17 :eAO4576.
33. Tamura R, Tanaka T, Miyake K, Tabei Y, Ohara K, Sampetrean O, et al. Histopathological investigation of glioblastomas resected under bevacizumab treatment. Oncotarget 2016;7(32):52423-35.
34. Manoharan S, Sindhu G, Nirmal M, Vetrichelvi V, Balakrishnan S. Protective effect of berberine on expression pattern of apoptotic, cell proliferative, inflammatory and angiogenic markers during 7, 12-dimethylbenz (a) anthracene induced hamster buccal pouch carcinogenesis. Pak J Biol Sci. 2011;14(20):918-32.
35. Gouda A, El-Didi F, Darwish Z, Zeitoun I. Expression of vascular endothelial growth factor in oral squamous cell carcinoma: a clinicopathological study. Alex Dent J. 2017;42(2):187-92
36. Martano M, Restucci B, Ceccarelli D, Lo Muzio L, Maiolino P. Immunohistochemical expression of vascular endothelial growth factor in canine oral squamous cell carcinomas. Oncol Lett. 2016;11(1):399-404.
37. Siva-Shankari S. Expression of Vascular Endothelial Growth Factor (VEGF-A) in Oral Submucous Fibrosis and Oral Squamous Cell Carcinoma: An Immunohistochemistry study. Masters thesis, Ragas Dental College and Hospital, Chennai.2018.
38. Araki-Maeda H, Kawabe M, Omori Y, Yamanegi K, Yoshida K, Yoshikawa K, et al. Establishment of an oral squamous cell carcinoma cell line expressing vascular endothelial growth factor a and its two receptors. J Dent Sci. 2022.
39. Astekar M, Joshi A, Ramesh G, Metgud R. Expression of vascular endothelial growth factor and microvessel density in oral tumorigenesis. J Oral Maxillofac Pathol. 2012;16(1):22-26.
40. Itashiki Y, Harada K, Takenawa T, Ferdous T, Ueyama Y, Mishima K. Antitumor effects of bevacizumab in combination with fluoropyrimidine drugs on human oral squamous cell carcinoma. Oncol Lett. 2021;22(4):730.
41. Ganjibakhsh M, Monshizadeh R, Nasimian A, Aminishakib P, Farzaneh P, Tavakoli S, et al. Anti-angiogenic efficacy of aflibercept and bevacizumab in primary oral squamous cell carcinoma cells. J Oral Pathol Med. 2018;47(6):575-82.
42. Chen D, Hurwitz H. Combinations of bevacizumab with cancer immunotherapy. Cancer J. 2018;24(4):193-204.
43. Yadav K, Lim J, Choo J, Ow S, Wong A, Lee M, et al. Immunohistochemistry study of tumor vascular normalization and anti-angiogenic effects of sunitinib versus bevacizumab prior to dose-dense doxorubicin/cyclophosphamide chemotherapy in HER2-negative breast cancer. Breast Cancer Res Treat. 2022;192(1):131-42.
44. Damiano V, Caputo R, Garofalo S, Bianco R, Rosa R, Merola G, et al. TLR9 agonist acts by different mechanisms synergizing with bevacizumab in sensitive and cetuximab-resistant colon cancer xenografts. Proc Natl Acad Sci U S A. 2007;104(30):12468-73.
45. Gajewski T. The next hurdle in cancer immunotherapy: overcoming the non–T-cell–inflamed tumor microenvironment. Semin Oncol. 2015;42(4):663-71.
46. Sharma P, Allison J. The future of immune checkpoint therapy. Science 2015;348(6230):56-61.
47. Sun H, Wang S, Yan S, Zhang Y, Nelson P, Jia H, et al. Therapeutic strategies targeting cancer stem cells and their microenvironment. Front Oncol. 2019;9:1104.
48. Economopoulou P, Kotsantis I, Psyrri A. Tumor microenvironment and immunotherapy response in head and neck cancer. Cancers 2020;12(11):3377.
49. Pisani L, Estadella D, Ribeiro D. The role of toll like receptors (TLRs) in oral carcinogenesis. Anticancer Res. 2017;37(10):5389-94.
50. Mäkinen L, Atula T, Häyry V, Jouhi L, Datta N, Lehtonen S, et al. Predictive role of Toll-like receptors 2, 4, and 9 in oral tongue squamous cell carcinoma. Oral Oncol. 2015;51(1):96-102.
51. Ren X, Wang F, Ji B, Gao C. TLR7 agonist induced repression of hepatocellular carcinoma via the TLR7-IKK-NF-κB-IL6 signaling pathway. Oncol Lett. 2016;11(5):2965-70.

52. Dias M, de Figueiredo B, Teixeira-Neto J, Guerra M, Fialho S, Cunha A. In vivo evaluation of antitumoral and antiangiogenic effect of imiquimod-loaded polymeric nanoparticles. Biomed Pharmacother 2018;103:1107-14.
53. Wu S, Zhao M, Sun Y, Xie M, Le K, Xu M, et al. The potential of Diosgenin in treating psoriasis: Studies from HaCaT keratinocytes and imiquimod-induced murine model. Life Sci. 2020;241:117115.
54. Fujimura T, Kambayashi Y, Fujisawa Y, Hidaka T, Aiba S. Tumor-associated macrophages: therapeutic targets for skin cancer. Front Oncol. 2018;8:3.
55. Vola M, Mónaco A, Bascuas T, Rimsky G, Agorio C, Chabalgoity J, et al. TLR7 agonist in combination with Salmonella as an effective antimelanoma immunotherapy. Immunotherapy 2018;10(8):665-79.
56. Vidovic D, Simms G, Pasternak S, Walsh M, Peltekian K, Stein J, et al. Case Report: Combined Intra-Lesional IL-2 and Topical Imiquimod Safely and Effectively Clears Multi-Focal, High Grade Cutaneous Squamous Cell Cancer in a Combined Liver and Kidney Transplant Patient. Front Immunol. 2021;12:678028.
57. Aspord C, Tramcourt L, Leloup C, Molens J, Leccia M, Charles J, et al. Imiquimod inhibits melanoma development by promoting pDC cytotoxic functions and impeding tumor vascularization. J Invest Dermatol. 2014t;134(10):2551-61.
58. Ren S, Wang Q, Zhang Y, Song Y, Dong X, Zhang W, et al. Imiquimod enhances the potency of an exogenous BM-DC based vaccine against mouse melanoma. Int Immunopharmacol. 2018;64:69-77.
59. Camargo L, Remiro P, Rezende G, Santos S, Franz-Montan M, Moraes Â. Development of bioadhesive polysaccharide-based films for topical release of the immunomodulatory agent imiquimod on oral mucosa lesions. Eur Polym J. 2021;151:110422.
60. Patinote C, Karroum N, Moarbess G, Cirnat N, Kassab I, Bonnet P, et al. Agonist and antagonist ligands of toll-like receptors 7 and 8: Ingenious tools for therapeutic purposes. Eur J Med Chem. 2020;193:112238.
61. Wester A, Eyler J, Swan J. Topical imiquimod for the palliative treatment of recurrent oral squamous cell carcinoma. JAAD Case Rep. 2017;3(4):329-31.
62. Mane S, Patilsoman B, Bhate P, Das D, Malusare P, Tomar N. To evaluate the efficacy and tolerability of topical 5% imiquimod in cases of oral leukoplakia: A pilot study. J Indian Acad Oral Med Radiol. 2021;33(1):27-31.
63. Guo X-l, Li D, Sun K, Wang J, Liu Y, Song J-r, et al. Inhibition of autophagy enhances anticancer effects of bevacizumab in hepatocarcinoma. J Mol Med. .2013;91(4):473-83.
64. Vinoth A, Kowsalya R. Chemopreventive potential of vanillic acid against 7, 12-dimethylbenz (a) anthracene-induced hamster buccal pouch carcinogenesis. J Cancer Res Ther. 2018;14(6):1285-90.
65. Ruiz-Villaverde R, Sanchez-Cano D, Burkhardt-Perez PJJotEAoD, Venereology. Superficial basal cell carcinoma treated with imiquimod 5% topical cream for a 4-week period: a case series. J Eur Acad Dermatol Venereol. 2009;23(7):828-31.
66. Yasuda S, Sho M, Yamato I, Yoshiji H, Wakatsuki K, Nishiwada S, et al. Simultaneous blockade of programmed death 1 and vascular endothelial growth factor receptor 2 (VEGFR2) induces synergistic antitumour effect in vivo. Clin Exp Immunol. 2013;172(3):500-6.
67. Silvan S, Manoharan S. Apigenin prevents deregulation in the expression pattern of cell-proliferative, apoptotic, inflammatory and angiogenic markers during 7, 12-dimethylbenz [a] anthracene-induced hamster buccal pouch carcinogenesis. Arch Oral Biol. 2013;58(1):94-101.
68. Faisal M, Abu Bakar M, Sarwar A, Adeel M, Batool F, Malik K, et al. Depth of invasion (DOI) as a predictor of cervical nodal metastasis and local recurrence in early-stage squamous cell carcinoma of oral tongue (ESSCOT). PLoS One. 2018;13(8):e0202632.
69. Weber M, Büttner-Herold M, Distel L, Ries J, Moebius P, Preidl R, et al. Galectin 3 expression in primary oral squamous cell carcinomas. BMC cancer 2017;17(1):906.